Seeing the Vibration from Fiber-Optic Cables: Rain Intensity Monitoring using Deep Frequency Filtering

Zhuocheng Jiang[1]* Yangmin Ding[1] Junhui Zhao[2] Yue Tian[1] Shaobo Han[1]
Sarper Ozharar[1] Ting Wang[1] James M. Moore[3]
[1]NEC Laboratories America, Inc [2]Eversource Energy [3]Verizon
{zhjiang, yding, ytian, shaobo, sarper, ting}@nec-labs.com junhui.zhao@eversource.com
james.m.moore@verizon.com

Abstract

The various sensing technologies such as cameras, LiDAR, radar, and satellites with advanced machine learning models offers a comprehensive approach to environmental perception and understanding. This paper introduces an innovative Distributed Fiber Optic Sensing (DFOS) technology utilizing the existing telecommunication infrastructure networks for rain intensity monitoring. DFOS enables a novel way to monitor weather condition and environmental changes, provides real-time, continuous, and precise measurements over large areas and delivers comprehensive insights beyond the visible spectrum. We use rain intensity as an example to demonstrate the sensing capabilities of DFOS system. To enhance the rain sensing performance, we introduce a Deep Phase-Magnitude Network (DFMN) divide the raw sensing data into phase and magnitude component, allowing targeted feature learning on each component independently. Furthermore, we propose a Phase Frequency learnable filter (PFLF) for the phase component filtering and conduct standard convolution layers on the magnitude component, leveraging the inherent physical properties of optical fiber sensing. We formulate the phase-magnitude channel into a parallel network and subsequently fuse the features for a comprehensive analysis in the end. Experimental results on the collected fiber sensing data show that the proposed method performs favorably against the state-of-the-art approaches.

1. Introduction

Optical fiber network, serving as the communication backbone, are extensively and densely deployed worldwide. The widespread of optical fiber infrastructures that telecom carriers have constructed over the past 30 years has been aimed to accommodating the surge in internet traffic and to facilitating the interconnections of 5G and future networks among cities, town, homes, and data centers. Distributed Fiber Optic Sensing (DFOS) technology leverages the existing fiber infrastructures as a potential sensing media [12, 32], enabling a wide-range, real-time, and continuous monitoring of surrounding environment perception without the need to introduce additional sensing devices. DFOS has been successfully employed in diverse applications including road traffic monitoring [22], intrusion detection [11, 16], earthquake detection [9], pipeline leakage monitoring [33] and structure change detection [1].

Operational telecom optical fiber cable networks hold substantial potential for environmental perception and sensing applications. DFOS technology transforms existing communication cables into individual sensors distributed every meter along the cable, with all the measurements being synchronized [12]. The basic principle behind the DFOS is that cable conditions such as a change of strain or temperature on the cable can influence the properties of the light signal traveling through an optical fiber. When pulsed light is launched into a sensing cable, a small fraction of light is backscattered and its properties are influenced by the fiber cable condition. The backscattered light includes three types of scattering: Raman scattering, Brillouin scattering, and Rayleigh scattering [12]. Figure 1 shows a schematic of distributed backscattering along the fiber cable and the scattering mechanisms inside the fiber cable. In this work we use a Phase-Optical Time Domain Reflectometer ϕ-OTDR method to detect backscattering lights. This methodology gauges alterations in the phase and amplitude of the Rayleigh backscattered signal via interferometric interrogation. As a result, the DFOS system retrieves the complex data from each location along the fiber cable with an impressive meter-level spatial resolution [13].

We employed a Distributed Acoustic Sensing (DAS) system utilize ϕ-OTDR detection. Figure 2 shows the DFOS system experimental setup, which comprising a DAS inter-

*: Corresponding author

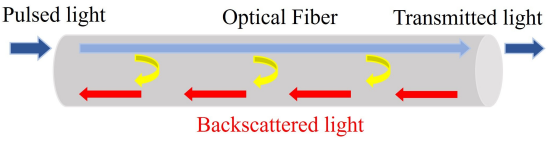

(a) Principle of backscattered light in an optical fiber

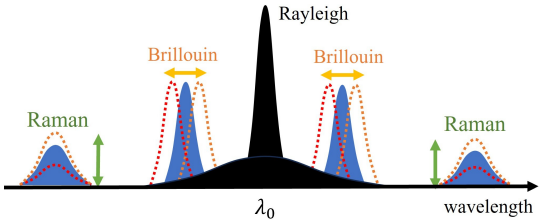

(b) Raman scattering, Brillouin scattering and Rayleigh scattering

Figure 1. Schematic of backscattering signals that are exploited in reflectometry based Distributed Fiber Optic Sensing (DFOS) system.

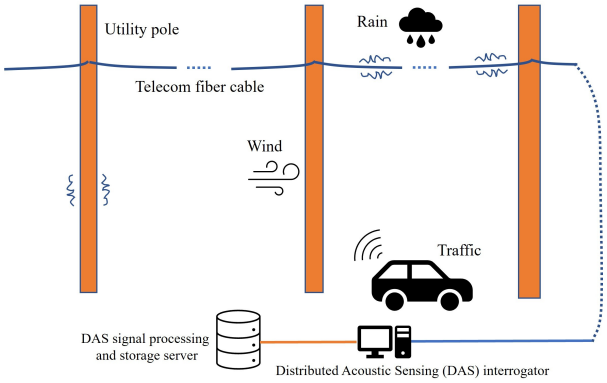

Figure 2. Distributed Fiber Optic Sensing (DFOS) system experiment setup by collecting Distributed Acoustic Sensing (DAS) to the aerial fiber cable for surrounding environmental monitoring.

rogator situated at control office, and a fiber cable with one end connected to a DAS to fortify environmental sensing. It is important to note that the collected raw data are complex numbers in the time domain, the phase response of the complex data in ϕ-OTDR systems refers to the change in the phase of the light signal that is scattered back to the detector as a result of interactions within the fiber. These phase changes are induced by external influences, such as mechanical strain, temperature variations, or acoustic vibrations. By measuring these phase changes, a ϕ-OTDR can provide detailed information about the environmental conditions along the length of the fiber. The fiber sensing data is continuously captured from 15 km of aerial fiber cable, at a sampling rate of 5 kHz, and at a spatial resolution of 1.2234 m.

Compared to camera-based imaging, Distributed Fiber Optic Sensing (DFOS) provides enhanced coverage for environmental monitoring across vast distances, offering detailed insights through vibration, acoustic, and temperature modalities that extend beyond the visible spectrum. This advantage inspires us to employ DFOS as a complement to camera-based imaging, as it captures a diverse range of physical parameters in various modalities, along with spatiotemporal data in a 2-dimensional (2D) format. Motivated by the studies that transform acoustic and vibration sensing data into 2D images [25, 40], our work similarly presents the fiber sensing data into 2D location-time matrices to enable more comprehensive analysis. Similar to natural images, adjacent spectrogram bins in fiber sensing data exhibit correlations in both time and spatial dimensions. This correlation renders convolutional neural networks (CNNs), traditionally used in computer vision tasks, well-suited for analyzing fiber sensing data. Moreover, similar to the representation of audio data in 2D formats, fiber sensing data also demonstrates additional correlations among frequencies that are harmonics of a base frequency. This phenomenon is attributed to the physical principles underlying acoustic production [23]. Considering the raw fiber sensing data matrix are complex numbers, we introduce a Deep Phase-Magnitude Network (DFMN) divide the raw data into phase and magnitude component, enabling targeted feature learning on each component independently. To capitalize on the inherent physical properties of fiber sensing data, we propose a Phase Frequency Learnable Filter (PFLF) dedicated to filtering the phase component, while conducting standard convolutional layers on the magnitude component. The main contributions of this work are summarized as follows:

1. We introduced a Distributed Fiber Optic Sensing (DFOS) solution for weather monitoring and environmental understanding. Compared to camera-based imaging, our solution offers extended monitoring coverage and provides rich information (vibration, acoustic, and temperature) across different modalities beyond the visible spectrum.
2. We showcase rain intensity monitoring as an illustrative example to demonstrate the environmental perception capabilities of DFOS. We introduce a Deep Phase-Magnitude Network (DPMN) to separate the raw data into phase and magnitude components, enabling targeted, fine-grained feature learning on each component independently.
3. We propose a Phase Frequency Learnable Filter (PFLF) dedicated to filtering the phase component. The PFLF module incorporates learnable filters to determine the frequency components crucial for rain intensity monitoring. Our analysis and experimental results demonstrate that the PFLF module achieves superior performance.

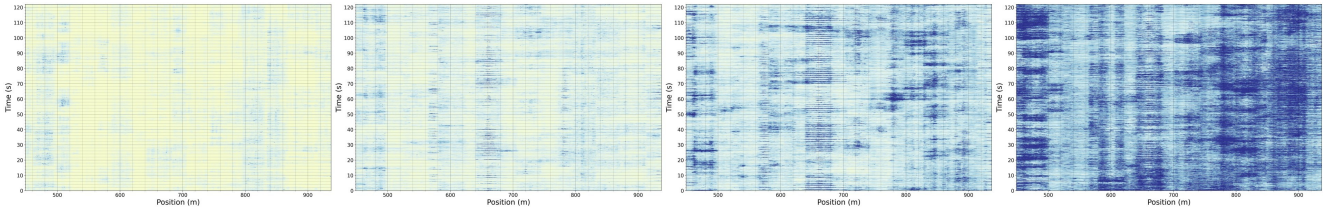

Figure 3. Visualization of the fiber sensing data in response to the increase of rain intensities. (a) Ambient data (No rain); (b) light rain; (c) Moderate rain; (d) Heavy rain. The raw fiber sensing data is captured over a two-minute duration with the fiber cable's location extending from 450m to 940m.

2. Related Works

Rain Intensity Monitoring. Rain detection and intensity monitoring are crucial for a wide range of scientific and industrial applications, such as transportation, agriculture, water management, weather forecasting, and building energy estimation. For instance, precipitation nowcasting provides high-resolution forecasting of rainfall and hydrometeors zero to two hours into the future, which is crucial for weather-dependent decision-making [24]. However, current methods depend on land-based weather stations and satellites are subject to limitations in terms of availability and accessibility. As climate change leads to more frequent and intense extreme precipitation events, there is an urgent need for improved methods to measure rainfall intensity accurately. This urgency highlights the imperative to innovate and develop sensors that are capable of long-range, wide-coverage rain data collection, thereby enhancing our ability to respond to and manage the impacts of these changes effectively. Various sensing technologies integrated with advanced deep convolution neural models [3, 8, 29], are specifically designed to enhance the precision of rain intensity monitoring. Notably, the deep ResNet framework can learn from the complex patterns in environmental data, making it highly effective for capturing the nuances of rain intensity [5, 26]. ConvLSTM offers an efficient way to process spatial data, which is essential when analyzing images or spatial patterns related to precipitation [4].

Additionally, radar-based rain sensor [10, 19], camera-based sensor [38], smart phones [7], satellite [6] and telecom fiber cables [5] have been effectively employed for rain intensity monitoring, significantly improving detection accuracy. In this paper, we aim to extract insights from fiber sensing data gathered through DFOS system to advance rain intensity monitoring. Figure 3 provides a visualization of phase response of complex fiber sensing data with the increasing rain intensities, captured over a two-minute duration with the fiber cable's location extending from 450m to 940m. The visualization clearly illustrates that the phase response of the raw data intensifies accordingly with the increase in rain intensity.

Learning in Frequency Domain. Frequency analysis has been widely used in conventional digital signal and image processing for decades. More recently, frequency domain filtering and transformer based on Fourier transform, has been incorporated into deep learning methods for solving different aspects of problems. Learned representations in the frequency domain contain rich pattern for image understanding tasks [34]. For instance, by separating invariant and specific components based on frequency prior knowledge, learning in the frequency domain enhances the trained model's generalization capabilities and minimizes the shift in model distribution [18, 30, 35, 36]. Augmenting data effectively in the frequency domain, frequency filtering improves the learning of informative representations of non-local receptive fields [2, 20, 27, 37]. Additionally, the straightforward application of the Fourier transform not only accelerates training but also facilitates the optimization of deep neural networks [15, 21, 28]. Prior research in frequency domain learning has revealed the different frequency components possess varying levels of importance during training, contributing distinctively to feature robustness.

Specifically, in [17], a light-weight layer is proposed to learn attention masks from the frequency representations after fast Fourier transform to enhance transferable components while suppressing the components not conducive to domain generalization. To solve the ineffective of transformer in de-blurred image, [14] proposed a discriminative frequency domain-based model, where a gated mechanism is utilized to discriminatively determine which low- and high-frequency information of the features should be preserved for latent clear image processing. In [31], authors designed two learnable frequency filters to extract domain-invariant spectrum and domain-specific spectrum, and a new instance-level contrastive loss to guide the network training. The success in frequency domain learning motivate us to further refine frequency domain analysis for fiber sensing data, aiming to automatically modulate various frequency components for enhanced performance.

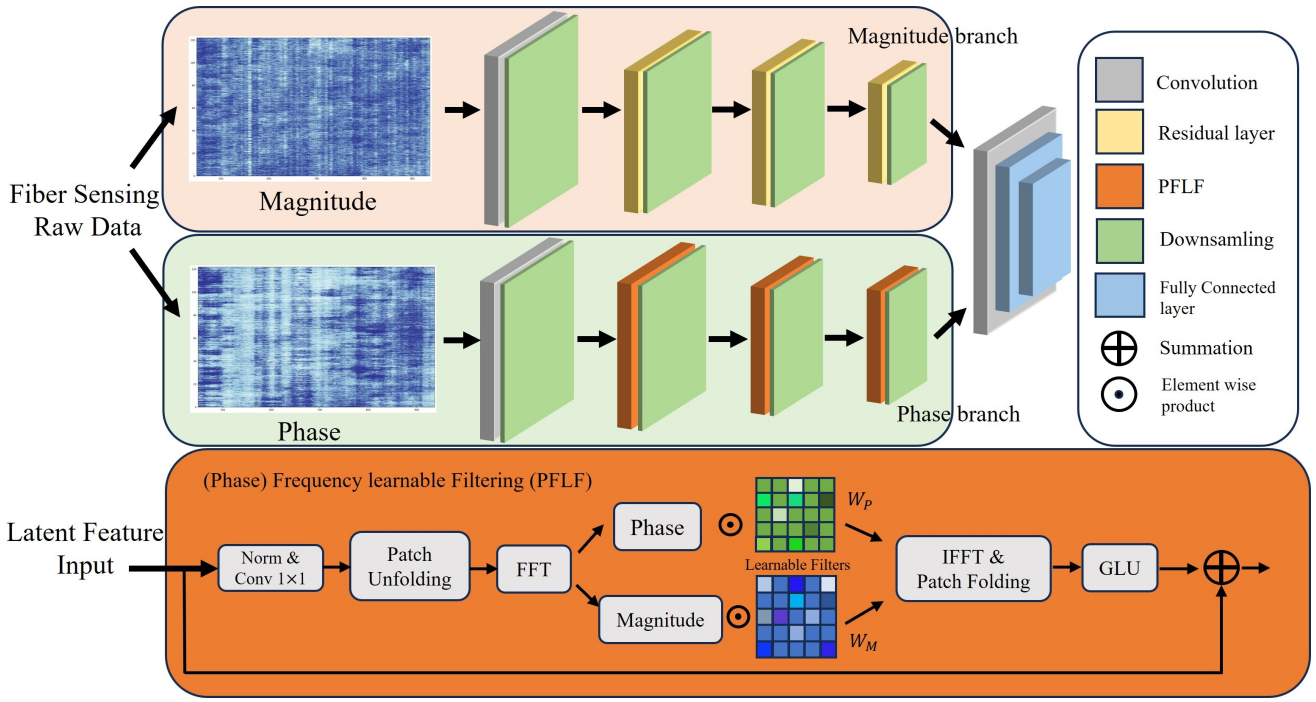

Figure 4. Overview of the proposed Deep Phase-Magnitude Network (DPMN). The DPMN consists of a magnitude component channel (the top branch) and a phase component channel (the second branch). The magnitude channel is designed to capture the amplitude information of raindrops impacting the fiber cable, while the phase channel concentrates on extracting the characteristics of how the impact of raindrops is transmitted through the fiber cables. We thus propose a Phase Frequency Learnable Filtering (PFLF) module (the bottom branch) delicate to phase channel.

3. Proposed Method

Our goal is to develop an effective and efficient method to explore the properties of frequency domain filtering for accurate rain monitoring and improve the domain generalization for environmental perception. By leveraging the inherent physical properties of DFOS fiber sensing data, we propose a Deep Phase-Magnitude Network (DFMN) divide the raw sensing data into phase and magnitude component, allowing targeted feature learning on each component independently. We introduce a Phase Frequency Learnable Filtering module (PFLF) specifically designed for filtering the phase component, while applying standard residual blocks to the magnitude component. We formulate the phase and magnitude branch as parallel networks, and eventually merging the features for an integrated analysis. Figure 4 provides an overview of our proposed methodology, with the specifics of each component detailed in the subsequent section.

3.1. Latent Frequency Learning Representations

Different from frequency-based signal or image processing methods that applied in the pixel space or original 1-D signals, we employ the proposed frequency filtering operations in the feature latent space. We briefly recall the conventional 2D Fast Fourier Transform (FFT) in image processing, and discuss the characteristics of applying it into latent feature representations.

Given the intermediate features of $\mathbf{X} \in \mathbb{R}^{C\times H\times W}$, where C, H and W are the channel, height and weight of the input feature X, we perform a 2D Fast discrete Fourier Transform (FFT) to these input features. This process yields the frequency representation $\mathbf{X^F} \in \mathbb{R}^{2C\times H\times \left(\lfloor \frac{W}{2} \rfloor +1\right)}$. The transformed $\mathbf{X^F}$ comprises $2C$ channels, incorporating both the real and imaginary parts. Leveraging the conjugate symmetric property of the FFT, $\mathbf{X^F}$ only needs retain the half of spatial dimensions thus has spatial resolution $H \times \left(\lfloor \frac{W}{2} \rfloor + 1\right)$. We express this FFT operation $\mathbf{X^F} = FFT\left(\mathbf{X}\right)$ as below:

$$\mathbf{X}^F\left(x,y\right) = \sum_{h=0}^{H-1}\sum_{w=0}^{W-1} \mathbf{X}\left(h,w\right) e^{-j2\pi\left(x\frac{h}{H}+y\frac{w}{W}\right)}. \quad (1)$$

In the frequency domain, the two primary components of $\mathbf{X}^F$ namely the magnitude component $\mathbf{X}_M$ and the phase component $\mathbf{X}_P$, can be obtained by:

$$\mathbf{X}_M^F = \sqrt{\mathbf{Re}\left\{\mathbf{X}^F\right\}^2 + \mathbf{Im}\left\{\mathbf{X}^F\right\}^2}, \quad (2)$$

$$\mathbf{X}_P^F = \arctan\left[\frac{\mathbf{Im}\left\{\mathbf{X}^F\right\}}{\mathbf{Re}\left\{\mathbf{X}^F\right\}}\right]. \tag{3}$$

where $\mathbf{Re}$ and $\mathbf{Im}$ correspond to the real and imaginary parts of $\mathbf{X}^F$, Benefiting from the FFT, these two components can capture the feature receptive field easily, which can just meet our need for efficient feature dependency modeling. The frequency representation $\mathbf{X}^F$ can be converted to the original feature space using an inverse FFT. This operation can be expressed as $\mathbf{X} = iFFT\left(\mathbf{X}^F\right)$:

$$\mathbf{X}\left(h,w\right) = \frac{1}{H\cdot W}\sum_{h=0}^{H-1}\sum_{w=0}^{W-1}\mathbf{X}^F\left(x,y\right)e^{j2\pi\left(x\frac{h}{H}+y\frac{w}{W}\right)}. \tag{4}$$

As discussed in [2, 14, 17], distinct frequency components of the original feature $\mathbf{X}$ are decomposed into elements across different spatial locations of $\mathbf{X}^F$, which can be regarded as a frequency-based disentanglement and reorganization of $\mathbf{X}$. This property not only makes learning in the frequency domain practically efficient, but also facilitates frequency filtering through simple designed learnable filters. An additional benefit is that $\mathbf{X}^F$ serves as a naturally global feature representation, which can facilitate the suppression of globally distributed domain-specific information, such as ambient noise and traffic noise, during data collection of the DFOS system.

3.2. Overview of Deep Phase-Magnitude Network

The raw fiber sensing data collected from the DFOS system comprise a complex number matrix, where the x-axis represents the range of cable locations, and the y-axis denotes the measurement time. It is important to note that this complex number matrix exists in the time domain, distinguishing it from complex numbers typically encountered in the frequency domain. Previous research on DFOS-based applications [11, 13] has focused exclusively on the phase component of the raw data, leading to the loss of signal intensity information related to the event. Here, we propose a Deep Phase-Magnitude Network (DPMN) designed to integrate both the phase and magnitude components of the data for more comprehensive learning. As shown in Figure 4, DPMN is structured with distinct branches for magnitude and phase.

Given that magnitude and phase represent distinct physical characteristics inherent to the DFOS system, we carefully design different learning modules for each of these two branches to ensure effective feature extraction of each data input. Let $\mathbf{S}$ be the raw data matrix collected from DFOS. This matrix can be decomposed into a magnitude response $\mathbf{S}_M = M\left(\mathbf{S}\right)$ and phase response $\mathbf{S}_P = P\left(\mathbf{S}\right)$ using Eq. 2 and Eq. 3, where $M(\cdot)$ and $P(\cdot)$ are operations to extract magnitude and phase, respectively.

The proposed DPMN utilizes standard residual convolutional blocks for feature learning on $\mathbf{S}_M$ within the time domain, and introduces a learnable filtering module dedicate to $\mathbf{S}_P$ in the frequency domain. The raindrops intensity information contained in the magnitude response renders it analogous to a 2-D intensity map, similar to those encountered in image processing. Thus we employ residual blocks within this branch to effectively process and analyze the data. On the other hand, the backscattering signal aberration such as phase leading or lagging caused by the difference locations of acoustic event, are captured by fiber cable and encapsulated within phase response. Correspondingly, we propose a Phase Frequency Learnable Filtering (PFLF) module for phase branch learning. Those two operations can be written as:

$$\mathbf{X}_M = ResBlock(\mathbf{S}_M), \tag{5}$$

$$\mathbf{X}_P = PFLF(\mathbf{S}_P), \tag{6}$$

where $\mathbf{X}_M$ and $\mathbf{X}_P$ represent the feature representations from the two branches, respectively. We merge these learned features into a unified feature representation, denoted as $(\mathbf{X}_M, \mathbf{X}_P)$. The integrated features contain global features from both magnitude and phase branches, providing a comprehensive representation of the raw fiber sensing data. In the end, the combined feature set is subsequently processed through a final convolutional block, employing a standard cross-entropy loss function to accurately assess the intensity range of the raindrops.

3.3. Frequency-based Learnable Filtering

In this subsection, we introduce the PFLF module for phase response channel, as illustrated in the bottom branch of Figure 4. Our goal is to adaptively select various frequency components within the feature representation space. We thus propose to employ a frequency learnable filtering on $\mathbf{X}_P$, enabling precise manipulation and enhancement of the signal characteristics pertinent to rain monitoring. Given input feature representation $\mathbf{X}_P$, we first applied a normalization layer followed by a 1×1 convolution layer, aim to enhance the reusability of feature maps and introduce additional non-linearities across different parts of the network. This feature pre-processing step can be written as:

$$\overline{\mathbf{X}}_P = Conv_{1\times 1}\left(\mathcal{N}(\mathbf{X}_P)\right). \tag{7}$$

We then apply a patch unfolding on the feature space, transforming the input feature maps into a series of smaller, overlapping patches. This process mainly utilized in vision transformers, allows the model to better exploit the local spatial relationships within the data, and learn more complex and hierarchical features [14, 39]. Following the unfolding of feature patches, a FFT operation, as specified in

Eq. 1, is applied to transform the phase response into the frequency domain:

$$\mathbf{X}_P^F = FFT(\mathcal{P}(\overline{\mathbf{X}}_P)), \tag{8}$$

where $\mathcal{P}$ is the patch unfolding operation. To enhance feature learning within the frequency domain, we decompose the frequency response into magnitude and phase using Eq. 2 and Eq. 3. Note this response analysis occurs within the frequency domain, distinguishing from the earlier discussed branch separation of raw fiber sensing data in time domain. Set $M(\mathbf{X}_P^F)$ and $P(\mathbf{X}_P^F)$ as the corresponding magnitude and phase, we multiply them element-wise with two learnable quantization matrices W_M and W_P. Subsequently, we integrate the filtered magnitude and phase responses to reconstruct the frequency domain's complex number matrix:

$$\begin{aligned}\overline{\mathbf{X}_P^F} = M(\mathbf{X}_P^F) \odot W_M \cdot cos(P(\mathbf{X}_P^F) \odot W_P) + \\ iM(\mathbf{X}_P^F) \odot W_M \cdot sin(P(\mathbf{X}_P^F) \odot W_P).\end{aligned} \tag{9}$$

Finally, we perform inverse FFT and patch folding $\mathcal{P}^{-1}(\cdot)$ to recover the frequency domain features to time domain:

$$\mathbf{X}_P^{'} = \mathcal{G}(\mathcal{P}^{-1}(iFFT(\overline{\mathbf{X}_P^F}))) + \mathbf{X}_P, \tag{10}$$

where $\mathcal{G}$ denotes Gated Linear Unit (GLU) function, we further enhance the process by adding the original input to the output of the frequency filtering, thereby aiming to facilitate more effective and robust feature selection.

4. Experiments

This section presents evaluations of the proposed method, including dataset description, implementation details, domain generalization results, ablation analysis on PFLF, and visualization analysis.

4.1. Dataset and parameter settings

Dataset. We perform experiments with the data collected from the field trials in the testbed using DFOS system. The dataset is collected along an optical route spanning over 15 km, with data collection operations running continuously in 24/7. Considering the large volume of collected data, we segment the raw data into small data matrices size 512×256. The ground truth of rain intensity is collected by a weather station that installed nearby the fiber cable. We separate the rain intensity into four categories based on the rain rate measured in inches per hour (in/h): Ambient condition (No rain), light rain ($0 \sim 0.1$ in/h), moderate rain ($0.1 \sim 0.3$ in/h) and heavy rain (above 0.3 in/h). Here we formulate rain monitoring as a classification problem rather than regression due to the discontinuous of the ground truth values from weather stations, particularly noting the presence of numerous missing values during data labeling. We choose five unique days from various seasons to enhance the diversity of the dataset, denoted as $\mathcal{D} = \{D_1, D_2, D_3, D_4, D_5\}$, which contains all categories of rain intensities. A total of over 8,000 raw data matrices are extracted for model training and evaluation.

Table 1. Performance comparisons of our proposed Phase Frequency Learnable Filter (PFLF) with baselines and other deep filtering models in the time domain and frequency domain. The "ResNet" refers to the vanilla residual network baseline. "FFC" refers to the frequency filtering solution proposed in [2], which incorporates ResNet-based frequency filtering techniques. "FSAS" and "DFFN" are frequency filtering modules introduced in [14].

Method	Accuracy	Precision	Recall	F1
ResNet [8]	0.922	0.902	**0.940**	0.920
FFC [2]	0.924	0.933	0.917	0.925
FSAS [14]	0.865	0.871	0.845	0.858
DFFN [14]	0.927	0.922	0.935	0.928
PFLF	**0.934**	**0.940**	0.932	**0.936**

Network architecture and parameter settings. As shown in the Figure 4, the magnitude and phase branch has symmetric architecture. Each branch contains a convolutional layer, succeeded by three network modules: residual blocks for the magnitude branch and PFLF modules for the phase branch. We use cross entropy loss function to constrain the network and train it using Adam optimizer with default parameters. The initial value of the learning rate is 10^{-3} and is updated with the cosine annealing strategy. The batch size is set to 16 and patch size for patch unfolding is set to 8 during training.

4.2. The effectiveness of PFLF

To investigate the effectiveness of the proposed PFLF module, we compare it with baseline ResNet [8] and other frequency filtering solutions FFC [2], FSAS [14], and DFFN [14]. Given that those models are applied across various tasks, we adapt these approaches to our scenario, maintaining an identical number of network layers to accelerate a fair comparison. Here we conduct the evaluation using the phase of the raw data, the network architecture is same as the phase branch as shown in Figure 4.

Table 1 presents the comparative analysis of the PFLF module against various baseline models. Clearly, our method surpasses the performance of other baselines, with PFLF achieving improvements in classification accuracy by 1.2%, 1.0%, 6.9%, and 0.7%, respectively. Notably, the superior performance of PFLF compared to ResNet demonstrates the advantage of frequency filtering over time-domain filtering in analyzing the phase response of raw data.

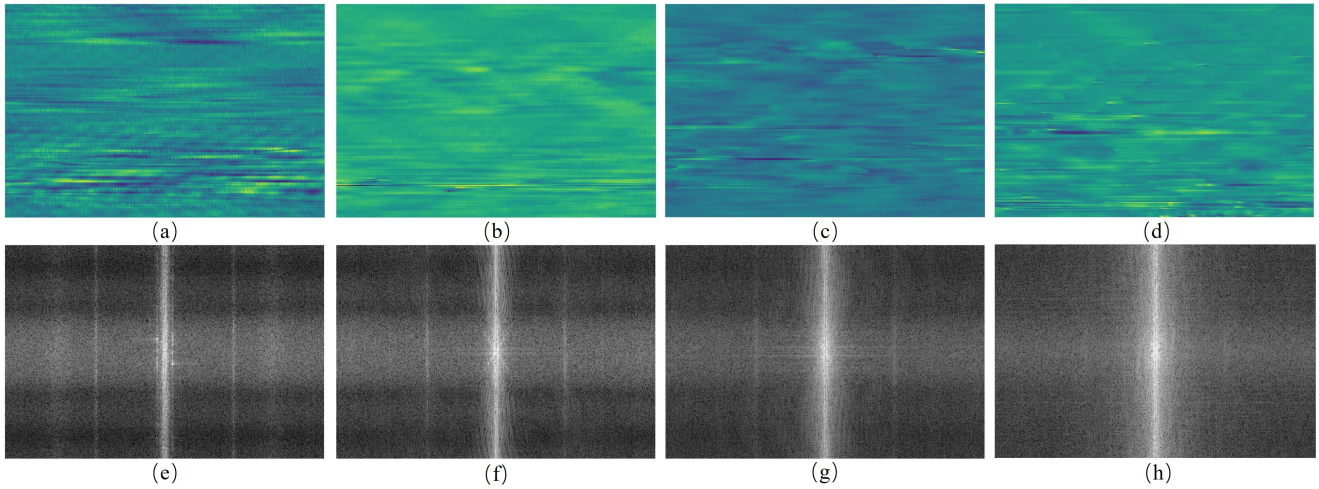

Figure 5. Comparison of phase response data patches alongside their corresponding frequency responses in feature space. Figure (a) $\sim$ (d) display the input patches with progressively increasing rain intensity from ambient to heavy. (a) No rain; (b) light rain; (c) Moderate rain; (d) Heavy rain. Figure (e) $\sim$ (h) depict the corresponding frequency responses of the patches above.

Table 2. Performance comparisons of domain generalization using proposed method and baseline models. The $\{D_1, D_2, D_3\}$ and $\{D_4, D_5\}$ represent the source domains and target domains, respectively.

Method	$\{D_1, D_2, D_3\} \rightarrow \{D_4, D_5\}$			
	Accuracy	Precision	Recall	F1
ResNet [8]	0.849	0.833	0.857	0.844
FFC [2]	0.925	0.927	0.911	0.919
FSAS [14]	0.849	0.863	0.855	0.859
DFFN [14]	0.921	0.916	**0.928**	0.922
PFLF	**0.932**	**0.944**	0.920	**0.932**

Table 3. Ablation study of filtering magnitude response in frequency domain and time domain. Here we use "ResNet" and "Frequency Learnable Filter (FLF)" as two baselines, where "M-" means magnitude of the raw data.

Method	Accuracy	Precision	Recall	F1
M-ResNet	**0.944**	**0.937**	**0.951**	**0.944**
M-FLF	0.913	0.912	0.897	0.904

4.2.1 Domain generalization of PFLF module

The baseline comparison given in the Table 1 aggregates all the data collected over five distinct days. However, in the real application scenario, it is crucial to depend on the model trained on previously collected data to predict current rain conditions. This requires the trained model exhibits strong generalization capabilities demonstrates resilience against diverse background conditions.

Here we formulate our problem within the context of domain generalization, categorizing the distinct days into source domains and target domains. The source and target domains may differ significantly due to various ambient sounds including wind and traffic. We regard $\{D_1, D_2, D_3\}$ as source domains, and set $\{D_4, D_5\}$ as target domain for evaluation. The experiment results are given in Table 2. Two key observations emerge from our results: (1) The PFLF outperforms other baseline models in terms of accuracy, demonstrating the efficacy of the proposed method in retaining general features to enhance classification accuracy. (2) Filtering in the frequency domain achieves consistent stability compared to time domain filtering when analyzing the phase response of raw data. For example, while conventional ResNet experiences a 7.3% drop in accurac but PFLF maintains stability.

Figure 5 shows the phase patch inputs and their corresponding frequency response in the feature space. Directly distinguishing the intensity differences of rain from the input phase patches (Figure 5 (a)$\sim$ (b)) is challenging; however, in Figure 5 (e) $\sim$ (h), the distinct patterns in frequency response become observable after applying the FFT transform, reflecting the variations in frequency components. For instance, in Figure 5 (e), the presence of bright vertical lines away from the center indicates high-frequency components. Conversely, Figure 5 (h) has a bright spot at the center of the frequency response denotes the dominance of low-frequency components. The central concentration observed in the frequency response may indicate that the fiber cable is detecting consistent and regular oscillations, potentially corresponding to the rhythmic impact of raindrops. Those transferable characteristics within the frequency domain of

Table 4. Performance comparisons of the proposed Deep Phase-Magnitude Network (DPMN) with baseline models including "MFCC-CNN" [26], "ResNet" [8], "FFC" [2], as well as "FSAS" and "DFFN" [14]. Domain generalization evaluations are provided in the right side of the table, with same experimental configuration as Table 2.

Method	Accuracy	Precision	Recall	F1	$\{D_1, D_2, D_3\} \rightarrow \{D_4, D_5\}$			
					Accuracy	Precision	Recall	F1
MFCC-CNN [26]	0.910	-	-	-	0.647	-	-	-
ResNet [8]	0.938	0.929	0.940	0.934	0.903	0.921	0.917	0.919
FFC [2]	0.953	0.942	**0.962**	0.951	0.942	0.937	0.944	0.940
FSAS [14]	0.879	0.884	0.863	0.873	0.886	0.863	0.892	0.877
DFFN [14]	0.946	0.952	0.933	0.942	0.938	0.921	**0.949**	0.935
DPMN	**0.961**	**0.954**	0.955	**0.954**	**0.950**	**0.942**	0.946	**0.944**

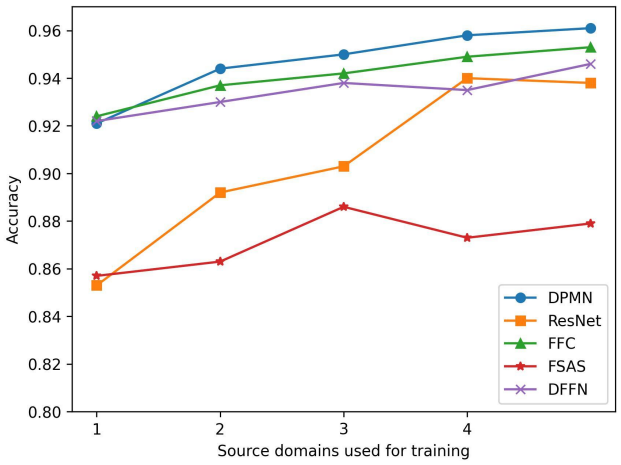

Figure 6. Classification accuracy variation with the increasing the source domain data for training. In x-axis, label "1" represents training with D_1 and testing with the remaining data, label "2" indicates training with $\{D_1, D_2\}$ and testing with the rest, and other labels follow this pattern.

phase patch inputs not only reinforce the interpretability of the data but also underscore the potential of a model to utilize these distinctive patterns to enhance domain generalization capabilities.

4.3. Experiments on DPMN model

This subsection we first conduct an ablation study on magnitude response, then we compare the proposed DPMN with other frequency filtering solutions to evaluate the classification performance.

4.3.1 Ablation study on magnitude response

To determine the most effective filtering solution for the magnitude response branch, we perform an ablation study comparing the impacts of frequency-domain filtering versus time-domain filtering. The findings, presented in Table 3, reveal that the conventional ResNet block consistently outperforms frequency-domain filtering. This suggests that time-domain feature extraction and selection play a more significant role than frequency-domain processing for the magnitude response. This critical insight informs our strategy to utilize distinct filtering methods for the phase and magnitude branches.

4.3.2 Evaluation on DPMN model

Table 4 presents the comparisons of the DPMN model with other models for the task of rain intensity classification. For a fair comparison, we have adapted other approaches into two branches architecture, same as DPMN solution. We observe the proposed solution outperforms other models in frequency filtering and time domain learning. Figure 6 presents the domain generalization results by gradually increase the data in source domain. These results demonstrate that our solution maintains stability against variations in the source domain.

5. Conclusion

In this paper, we introduce a Deep Phase-Magnitude Network (DFMN) and point out that combining the filtering in time domain and frequency domain can significantly enhance the classification accuracy and improve the domain generalization ability. We divide the raw fiber sensing data into magnitude response and phase response for parallel feature representation learning. Furthermore, we propose a Phase Frequency Learnable Filter (PFLF) specifically designed for phase component learning, which effectively determines the frequency components crucial for enhancing rain detection accuracy. In the end, we formulate the phase-magnitude channel within a dual-path network and subsequently fuse the features for a comprehensive analysis. Extensive experiments and ablation studies demonstrate the effectiveness of our proposed method.

References

[1] Filippo Bastianini, Andrea Rizzo, Nestore Galati, Ursula Deza, and Antonio Nanni. Discontinuous brillouin strain monitoring of small concrete bridges: comparison between near-to-surface and smart FRP fiber installation techniques. In *Sensors and Smart Structures Technologies for Civil, Mechanical, and Aerospace Systems*, pages 612—-623, 2005. 1

[2] Lu Chi, Borui Jiang, and Yadong Mu. Fast fourier convolution. In *NeurIPS*, pages 4479—-4488, 2020. 3, 5, 6, 7, 8

[3] Francois Chollet. Xception: Deep learning with depthwise separable convolutions. In *CVPR*, pages 1251–1258, 2017. 3

[4] Codrut-Andrei Diaconu, Sudipan Saha, Stephan Günnemann, and Xiaoxiang Zhu. Understanding the role of weather data for earth surface forecasting using a convlstm-based model. In *CVPR Workshop*, pages 1362–1371, 2022. 3

[5] Yangmin Ding, Yue Tian, Sarper Ozharar, Zhuocheng Jiang, and Ting Wang. Rain intensity detection and classification with pre-existing telecom fiber cables. In *Optical Sensors and Sensing Congress*, pages 1–3, 2022. 3

[6] Gianluigi Folino, Massimo Guarascio, and Francesco Chiaravalloti. Learning ensembles of deep neural networks for extreme rainfall event detection. *Neural Computing and Applications*, 35:10347—-10360, 2023. 3

[7] Hansong Guo, He Huang, Yu-E Sun, Youlin Zhang, Shigang Chen, and Liusheng Huang. Chaac: Real-time and fine-grained rain detection and measurement using smartphones. *IEEE Internet of Things Journal*, 6(1):997–1009, 2019. 3

[8] Kaiming He, Xiangyu Zhang, Shaoqing Ren, and Jian Sun. Deep residual learning for image recognition. In *CVPR*, pages 770–778, 2016. 3, 6, 7, 8

[9] Pablo D. Hernández, Jaime A. Ramírez, and Marcelo A. Soto. Deep-learning based earthquake detection for fiber-optic distributed acoustic sensing. *Journal of Lightwave Technology*, 40(8):2639–2650, 2022. 1

[10] Papat Hidayatulloh, B. Berlian Surya Wicaksana, Syukri Darmawan, Annida Rahmawati, Tiin Sinatra, and Asif Awaludin. An improved rainfall detection of rain radar using high-precision circuit and speckle filtering. In *International Conference on Radar, Antenna, Microwave, Electronics, and Telecommunications*, pages 123–127, 2022. 3

[11] Ming-Fang Huang, Jian Fang, Shaobo Han, Zhuocheng Jiang, Sarper Ozharar, Yuheng Chen, Tomoyuki Hino, and Ting Wang. Field tests of impulsive acoustic event detection, localization, and classification over telecom fiber networks. In *OptoElectronics and Communications Conference (OECC)*, pages 1–3, 2022. 1, 5

[12] Ezra Ip, Jian Fang, Yaowen Li, Qiang Wang, Ming-Fang Huang, Milad Salemi, and Yue-Kai Huang. Distributed fiber sensor network using telecom cables as sensing media: technology advancements and applications. *Journal of Optical Communications and Networking*, 14(1):A61–A68, 2022. 1

[13] Zhuocheng Jiang, Yue Tian, Yangmin Ding, Sarper Ozharar, and Ting Wang. Utility polelocalization by learning from ambient traces on distributed acoustic sensing. In *ICASSP*, pages 1–5, 2023. 1, 5

[14] Lingshun Kong, Jiangxin Dong, Jianjun Ge, Mingqiang Li, and Jinshan Pan. Efficient frequency domain-based transformers for high-quality image deblurring. In *CVPR*, pages 5886–5895, 2023. 3, 5, 6, 7, 8

[15] Shaohua Li, Kaiping Xue, Bin Zhu, Chenkai Ding, Xindi Gao, David Wei, and Tao Wan. Falcon: A fourier transform based approach for fast and secure convolutional neural network predictions. In *CVPR*, pages 8705—-8714, 2020. 3

[16] Zhongqi Li, Jianwei Zhang, Maoning Wang, Yuzhong Zhong, and Fei Peng. Fiber distributed acoustic sensing using convolutional long short-term memory network: a field test on high-speed railway intrusion detection. *Opt Express.*, 28(3):2925–2938, 2020. 1

[17] Shiqi Lin, Zhizheng Zhang, Zhipeng Huang, Yan Lu, Cuiling Lan, Peng Chu, Quanzeng You, Jiang Wang, Zicheng Liu, Amey Parulkar, Viraj Navkal, and Zhibo Chen. Deep frequency filtering for domain generalization. In *CVPR*, pages 11797–11807, 2023. 3, 5

[18] Quande Liu, Cheng Chen, Jing Qin, Qi Dou, and Pheng-Ann Heng. Feddg: Federated domain generalization on medical image segmentation via episodic learning in continuous frequency space. In *CVPR*, pages 1013—1023, 2021. 3

[19] Zhizhong Lu, Lei Sun, and Ying Zhou. A method for rainfall detection and rainfall intensity level retrieval from x-band marine radar images. *Applied Sciences*, 11(4):1565–4366, 2021. 3

[20] Xintian Mao, Yiming Liu, Wei Shen, Qingli Li, and Yan Wang. Deep residual fourier transformation for single image deblurring. In *arXiv preprint arXiv:2111.11745*, 2021. 3

[21] Michael Mathieu, Mikael Henaff, and Yann LeCun. Fast training of convolutional networks through ffts. In *arXiv preprint arXiv:1312.5851*, 2013. 3

[22] Chaitanya Narisetty, Tomoyuki Hino, Ming-Fang Huang, Ryusuke Ueda, Hitoshi Sakurai, Akihiro Tanaka, Takashi Otani, and Toru Ando. Overcoming challenges of distributed fiber-optic sensing for highway traffic monitoring. *Journal of the Transportation Research Board*, 2675(2):233–242, 2021. 1

[23] Hendrik Purwins, Bo Li, Tuomas Virtanen, Jan Schluter, Shuo-Yiin Chang, and Tara Sainath. Deep learning for audio signal processing. *IEEE JOURNAL OF SELECTED TOPICS IN SIGNAL PROCESSING*, 13(2):206–219, 2019. 2

[24] Suman Ravuri, Karel Lenc, Matthew Willson, Dmitry Kangin, Remi Lam, Piotr Mirowski, Megan Fitzsimons, Maria Athanassiadou, Sheleem Kashem, Sam Madge, Rachel Prudden, Amol Mandhane, Aidan Clark, Andrew Brock, Karen Simonyan, Raia Hadsell, Niall Robinson, Ellen Clancy, Alberto Arribas, and Shakir Mohamed. Skilful precipitation nowcasting using deep generative models of radar. *Nature*, 597:672–677, 2021. 3

[25] Mark Sheinin, Dorian Chan, Matthew O'Toole, and Srinivasa G. Narasimhan. Dual-shutter optical vibration sensing. In *CVPR*, pages 16324–16333, 2022. 2

[26] Sai Shi, Yangmin Ding, Yue Tian, Zhuocheng Jiang, Sarper Ozharar, Ting Wang, and James M. Moore. Beyond communication: Telecom fiber networks for rain detection and classification. In *International Conference on Optical Fiber Sensors (OFS)*, pages 1–4, 2023. 3, 8

[27] Roman Suvorov, Elizaveta Logacheva, Anton Mashikhin, Anastasia Remizova, Arsenii Ashukha, Aleksei Silvestrov, Naejin Kong, Harshith Goka, Kiwoong Park, and Victor Lempitsky. Resolution-robust large mask inpainting with fourier convolutions. In *WACV*, pages 2149—2159, 2022. 3

[28] Keivan Alizadeh Vahid, Anish Prabhu, Ali Farhadi, and Mohammad Rastegari. Butterfly transform: An efficient fft based neural architecture design. In *CVPR*, pages 12024––12033, 2020. 3

[29] Ashish Vaswani, Noam Shazeer, Niki Parmar, Jakob Uszkoreit, Llion Jones, Aidan N. Gomez, Lukasz Kaiser, and Illia Polosukhin. Attention is all you need. In *NIPS*, pages 1251–1258, 2017. 3

[30] Jingye Wang, Ruoyi Du, Dongliang Chang, Kongming Liang, and Zhanyu Ma. Domain generalization via frequency-domain-based feature disentanglement and interaction. In *CVPR*, pages 4821—-4829, 2022. 3

[31] Kunyu Wang, Xueyang Fu, Yukun Huang, Chengzhi Cao, Gege Shi, and Zheng-Jun Zha. Generalized uav object detection via frequency domain disentanglement. In *CVPR*, pages 1064–1073, 2023. 3

[32] Glenn A. Wellbrock, Tiejun J. Xia, Ming-Fang Huang, Milad Salemi, Yaowen Li, Philip N. Ji, Sarper Ozharar, Yuheng Chen, Yangmin Ding, Yue Tian, Ting Wang, and Yoshiaki Aono. Field trial of distributed fiber sensor network using operational telecom fiber cables as sensing media. In *European Conference on Optical Communications*, pages 1–3, 2020. 1

[33] Huijuan Wu, Jiping Chen, Xiangrong Liu, Yao Xiao, Mengjiao Wang, Yi Zheng, and Yunjiang Rao. One-dimensional CNN-based intelligent recognition of vibrations in pipeline monitoring with DAS. *Journal of Lightwave Technology*, 37(17):4359–4366, 2019. 1

[34] Kai Xu, Minghai Qin, Fei Sun, Yuhao Wang, Yen-Kuang Chen, and Fengbo Ren. Learning in the frequency domain. In *CVPR*, pages 1740–1749, 2020. 3

[35] Qinwei Xu, Ruipeng Zhang, Ya Zhang, Yanfeng Wang, and Qi Tian. A fourier-based framework for domain generalization. In *CVPR*, pages 14383—14392, 2021. 3

[36] Yanchao Yang and Stefano Soatto. Fda: Fourier domain adaptation for semantic segmentation. In *CVPR*, pages 4085—4095, 2020. 3

[37] Dong Yin, Raphael Gontijo Lopes, Jon Shlens, Ekin Dogus Cubuk, and Justin Gilmer. A fourier perspective on model robustness in computer vision. In *NeurIPS*, pages 1–11, 2019. 3

[38] Hang Yin, Feifei Zheng, Huan-Feng Duan, Dragan Savic, and Zoran Kapelan. Estimating rainfall intensity using an image-based deep learning model. *Research Hydraulic Engineering*, 21(4):162–174, 2023. 3

[39] Kai Zhang, Luc Van Gool, and Radu Timofte. Deep unfolding network for image super-resolution. In *CVPR*, pages 3217–3226, 2020. 5

[40] Andrea Zunino, Marco Crocco, Samuele Martelli, Andrea Trucco1, Alessio Del Bue, and Vittorio Murino. Seeing the sound: a new multimodal imaging device for computer vision. In *ICCV Workshop*, pages 6–14, 2015. 2